ACS APPLIED MATERIALS & INTERFACES

Research Article

www.acsami.org

Biotemplated Fabrication of Sn@C Anode Materials Based on the Unique Metal Biosorption Behavior of Microalgae

Xinyong Tao, Rui Wu, Yang Xia, Hui Huang, Weicong Chai, Tong Feng, Yongping Gan, and Wenkui Zhang*

College of Materials Science and Engineering, Zhejiang University of Technology, Hangzhou 310014, People's Republic of China

Supporting Information

ABSTRACT: Biotemplating is an effective strategy to obtain morphology-controllable materials with structural specificity, complexity, and corresponding unique functions. Different from traditional biotemplating strategies replicating the morphology and using biogenic elements of biomaterials (e.g., C, Si, N, Fe, P, S), we take advantage of the unique heavy-metal-ion biosorption behavior of microalgae to fabricate tin-decorated carbon (Sn@C) anode materials for lithium-ion batteries. Microalgae *Spirulina platensis* is used as the biotemplate, the renewable carbon source, and the biosorbent. After a facile one-step heat treatment, Sn@C with tin particles (20−30 nm) dispersing into the porous carbon matrix can be obtained. Fourier transform infrared spectra reveal that metal-ion biosorption results from the complexation reactions between Sn^{4+} ions and the hydroxyl groups associated with alginate. The Sn@C anode shows a discharge capacity of 520 mAh g^{-1} after 100 cycles, as well as excellent cycle stability and high coulombic efficiency (approximately 100%), exhibiting fascinating electrochemical performance. This facile, green, and economical strategy not only will extend the scope of biotemplating synthesis of functional materials but also will provide reference for environmental protection and water purification.

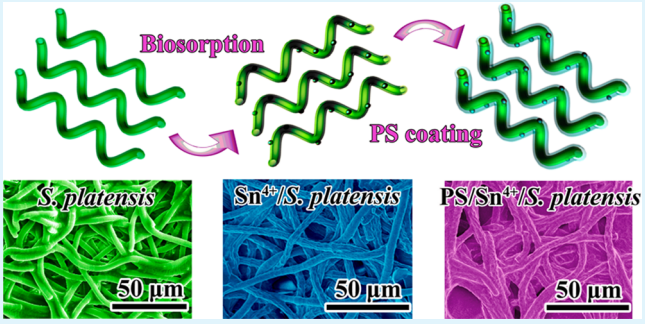

KEYWORDS: *microalgae, biotemplate, tin, anode, lithium-ion batteries*

INTRODUCTION

The need for renewable, sustainable energy, along with the aspiration to lower greenhouse gas emissions and decrease our dependency on fossil fuels, has driven interest and research toward the development of rechargeable lithium-ion batteries (LIBs) with high storage capacity and cycling stability.[1−8] As the anode material for LIBs, metallic tin has emerged as a topic of growing interest in the energy field because of its special advantages. First, its theoretical capacity (993 mAh g^{-1} or 7313 mAh cm^{-3}) based on one tin atom can maximally react with 4.4 lithium atoms to form a $Li_{4.4}Sn$ alloy is significantly higher than that of commercial graphite (LiC_6, 372 mAh g^{-1} or 833 mAh cm^{-3}).[3,4,9−17] Crystallographic studies suggested that the realistic form of this end phase could be $Li_{17}Sn_4$ (thus, 4.25 lithium per tin). Therefore, its maximum gravimetric capacity could be 959.5 mAh g^{-1}, which is still much higher than that of most common graphite anodes.[18,19] Second, the tin anode has higher operating voltage than graphite; thus, it is less reactive and has high safety ratings during repeated charge/discharge cycles.[9] Third, an important advantage of metallic tin over graphite is that it does not suffer from solvent intercalation, which causes irreversible charge losses.[9,20] However, the large amount of lithium insertion/extraction causes a severe volume change (300%), which leads to pulverization of tin particles and a loss of contact with the current collector, resulting in a rapid capacity decay.[2,13,15,21]

To tackle this problem, much effort has been devoted to optimizing the morphology, composition, structure, conductivity, and surface chemistry of tin anode materials for high-performance LIBs. The most effective methods include (a) reducing the tin particle size to nanoscale to efficiently alleviate the absolute strain induced by the large volume change during charge/discharge processes and moderate particle pulverization,[2] (b) introducing a lithium-inactive element (M) to the metallic tin phase to form a SnM-type electrode, in which the inactive M formed during lithiation/delithiation can buffer the volume expansion of the tin phase,[22] (c) uniformly dispersing tin particles into a conductive carbon matrix to confine volume change and maintain the mechanical integrity of the composite electrode.[2,5] Obviously, fabricating the Sn/C composite is an effective and ideal strategy to improving the electrochemical performance of tin anodes. To date, the approach to fabricating the Sn/C composite can be generally divided into four aspects: (a) chemical reduction;[23−25] (b) chemical vapor deposition;[26−30] (c) pyrolysis;[5,31−33] (d) template techniques.[14,26]

Compared with the above methods, the biotemplating technique is an impressive strategy to achieving morphology-controllable materials with structural specialty, complexity, and

Received: January 2, 2014
Accepted: February 11, 2014
Published: February 11, 2014

relevant fascinating functions derived from biomaterials.[34] Many state-of-art microstructures have been well-established using a wide range of biotemplates with multiscale structures and novel morphologies, which can enhance the performance of the objected materials. Recently, our group demonstrated that the rational utilization of the biotemplating strategy can realize advanced functional materials including phosphates, oxides, and carbides by using a variety of biotemplates, such as bamboo,[35−37] pollen grains,[38] cotton fibers,[39] microalgae,[40,41] etc. However, these conventional biotemplating methods focus only on the replicating of the morphology and using biogenic elements of biomaterials (e.g., C, Si, N, Fe, P, S), and the biofunctionality of the biological systems was seriously neglected. For example, microalgae, consisting of a high amount of protein, polysaccharide (alginate, etc.), and other lipids, possess a variety of functional groups that can absorb and uptake heavy-metal ions.

Herein, we take advantage of the unique biosorption behavior of microalgae to fabricate Sn@C anode materials using *Spirulina platensis* as the biotemplate, the biosorbent, and the renewable carbon source. The obtained Sn@C composite, in which tin nanoparticles (20−30 nm in diameter) were uniformly embedded in the porous carbon matrix, exhibited excellent cycling stability and rate performance in LIBs. It is believed that this green, facile, and convenient biotemplate method will open up new routes toward synthesizing other new advanced functional materials.

EXPERIMENTAL SECTION

Materials Synthesis. All chemicals were of analytical grade and were used as received without further purification. The Sn@C composite with tin particles inserted in the porous carbon matrix was fabricated via a facile biosorption and subsequent calcination procedure. To start with, 0.315 g of $SnCl_4{\cdot}5H_2O$ was dissolved in absolute ethanol to form a 0.4 M precursor solution. Meanwhile, *S. platensis* was washed several times by formaldehyde and deionized water (1:1 by volume) to remove unwanted materials. Then *S. platensis* was added to the above precursor solution. After 1 h at room temperature, the mixture was filtered, dried at 80 °C, and then immersed in 10 wt % polystyrene (PS) dissolved in dimethylformamide. Finally, the sample was calcined in a tube furnace at 600 °C for 3 h under a flowing nitrogen atmosphere to obtain black resulting materials (noted as sample A3). For comparison, the pristine *S. platensis* (A1) and tin-metal-ion-adsorbed *S. platensis* without a PS coating film (A2) were calcined at the same conditions to obtain the control samples. These final products were ground to fine powders and used as anode materials in LIBs.

Characterization. X-ray diffraction (XRD) of the samples was conducted by an X'Pert Pro diffractometer using Cu Kα radiation (λ = 0.15418 nm). The morphology of the samples was characterized by scanning electron microscopy (SEM; Hitachi S4700) and transmission electron microscopy (TEM; FEI Tecnai G2 F30). Fourier transform infrared radiation (FT-IR) was performed in air using the KBr pellet method by a infrared spectrophotometer (Nicolet 6700). Thermogravimetric analysis (TGA) was evaluated in an air atmosphere by using a thermogravimetric analyzer (Mettler Toledo) operated at a heating rate of 10 °C min^{-1} from room temperature to 700 °C. The Raman spectrum was performed on a Renishaw InVia Raman spectrometer under a backscattering geometry (λ = 532 nm). Nitrogen adsorption−desorption was determined by Brunauer−Emmett−Teller (BET) tests using an ASAP 2020 instrument (Micromeritics Instruments). The KBr pellet method was used to prepare the sample for FT-IR analysis. For TEM measurement after cycling, the cell charged to 2.7 V after 100 cycles was disassembled with pliers. The working electrode was immersed in absolute alcohol with ultrasonication. Then the solution was washed several times by absolute alcohol. After being dried at room temperature, the final black powders were used for TEM observation.

Electrochemical Measurements. Electrochemical characterization of the Sn@C composite was carried out with the CR2025 coin-type cell using lithium foil as the counter electrode. The testing electrode was fabricated by mixing active materials, conductivity agent (Super P), and poly(vinylidene fluoride) binder at a weight ratio of 70:15:15 in a *N*-methyl-2-pyrrolidene solvent. After the testing electrodes were dried at 80 °C under vacuum overnight, the coin cells were assembled inside an argon-filled glovebox. The electrolyte was 1 M $LiPF_6$ in ethylene carbonate−dimethyl carbonate (1:1 by volume), and the separator was a polypropylene membrane. The galvanostatical charge (Li^+ extraction) and discharge (Li^+ insertion) were conducted in the voltage range of 0.005−2.7 V versus Li/Li^+ at different current densities using a Battery Testing System at ambient temperature (Shenzhen Neware Battery, China). Cyclic voltammetry (CV) curves were measured at a scanning rate of 0.1 mV s^{-1} within the potential range of 0.005−2.7 V versus Li/Li^+ using a CHI660D electrochemistry working station (Shanghai Chenhua, China).

RESULTS AND DISCUSSION

The main process of fabricating the Sn@C composite is shown schematically in Figure 1. First, *S. platensis* is immersed in the

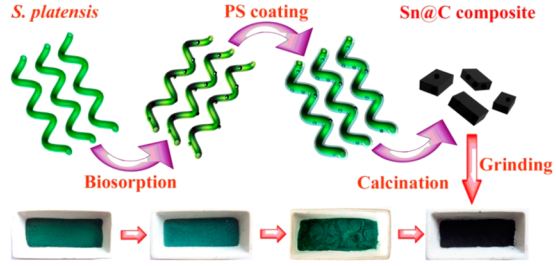

Figure 1. Schematic illustration of the preparation process of the Sn@C composite.

tin precursor to finish the biosorption procedure. In order to ensure that tin particles could be strongly anchored to the carbon matrix, the PS film is coated onto the surface of *S. platensis* after biosorption. During subsequent heat treatment, the carbonaceous compounds in *S. platensis* and PS decompose to carbon, as well as form a series of gaseous products (such as CO, H_2, CH_4, and C_2H_4)[42] to act as a reducing atmosphere, which can transform SnO_2 to tin. Finally, these tin nanocrystals are successfully dispersed into carbonaceous matrixes and constitute the Sn@C composite.

It is well-known that many algaes can capture and adsorb heavy-metal ions, which show fascinating potential applications in environmental protection and water purification.[43−45] However, there is some debate about the detailed biosorption mechanisms. Fourest and Volesky demonstrated that carboxyl groups of alginate play a major role in the complexation of heavy metals (Cd and Pb) by dead biomass of the brown seaweed *Sargassum fluitans*.[46] An ion-exchange biosorption mechanism was also suggested by Schiewer and Volesky.[47] Arief et al. highlighted the fact that carboxyl, hydroxyl, and amide groups are all engaged in the adsorption of metals using FT-IR analysis.[48] In our case, FT-IR was performed to investigate the biosorption mechanisms of *S. platensis*. The FT-IR transmission spectra before and after biosorption of Sn^{4+} ions onto *S. platensis* are shown in Figure 2. From the curve of pristine algae before adsorption, the major intense bands are around 3421, 2925, 2851, 2362, 1652, 1542, 1244, 1029, and 668 cm^{-1}. The O−H bond stretching can be observed centered

dx.doi.org/10.1021/am500020e | ACS Appl. Mater. Interfaces 2014, 6, 3696−3702

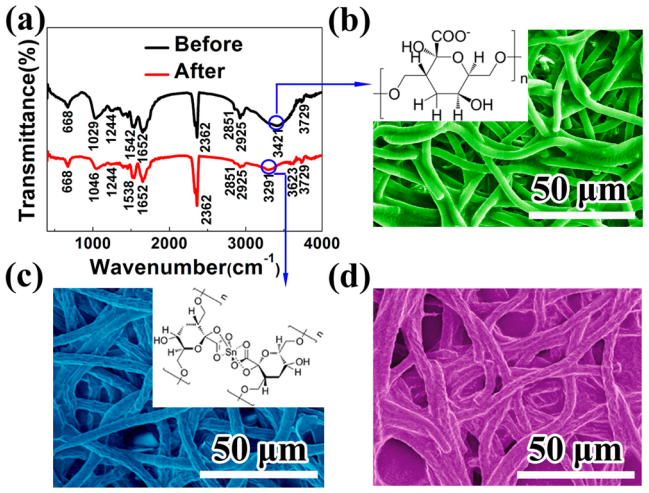

Figure 2. (a) FT-IR spectra of before and after adsorption. (b) SEM image of live *S. platensis*. (c) SEM image of Sn^{4+}-ion-adsorbed *S. platensis*. (d) SEM image of adsorbed *S. platensis* with a PS coating layer. The inset images in parts b and c are biomolecular structures of alginate before and after adsorption, respectively.

at 3421 cm^{-1}.[49] The peaks in the region of 3000−2850 cm^{-1} are assigned to the aliphatic C−H stretching vibrations of −CH, $-CH_2$, and $-CH_3$. The scissor bending of NH_2 groups can be detected at 2362 and 1652 cm^{-1}. C═C stretching at 1542 cm^{-1} can be observed. The bands at 1029 cm^{-1} can be attributed to C−N stretching of proteins.[50] The FT-IR spectrum of *S. platensis* exposed to Sn^{IV} ions displays no shift or change in most of the characteristic absorbance bands with the exception of a strong peak shift at 3291 and 1046 cm^{-1}, indicating that both the hydroxyl groups of the alginate and the C−N stretching of proteins play key roles in the biosorption process. On the basis of our experimental results, the biomolecular structures of alginate before and after adsorption (the inset in Figure 2b,c) are depicted to explain complexation between the hydroxyl groups and tin metal ions.

The corresponding SEM images of the precursors were taken to show the surface morphology. Figure 2b displays the SEM image of algae before adsorption, showing a diameter ranging from 5 to 8 μm. As shown in Figure 2c, the morphologies of tin-metal-ion-absorbed *S. platensis* are well maintained. However, *S. platensis* after Sn^{4+} adsorption displays a coarse surface and a larger size than that of the pristine sample. Similar results have been reported by Arief et al. They found that the algae cell surface was different and became wrinkled after adsorption of Cr^{3+}, indicating that the primary Cr^{III} sequestering sites were on the cell wall surface instead of the intracellular sites.[48] This phenomenon gives direct evidence of the biosorption behavior. Compared with Figure 2c, there was no obvious change in the diameter and the morphology of adsorbed *S. platensis* after PS coating (Figure 2d), indicating that the thin PS layer has been coated on the surface of algae uniformly.

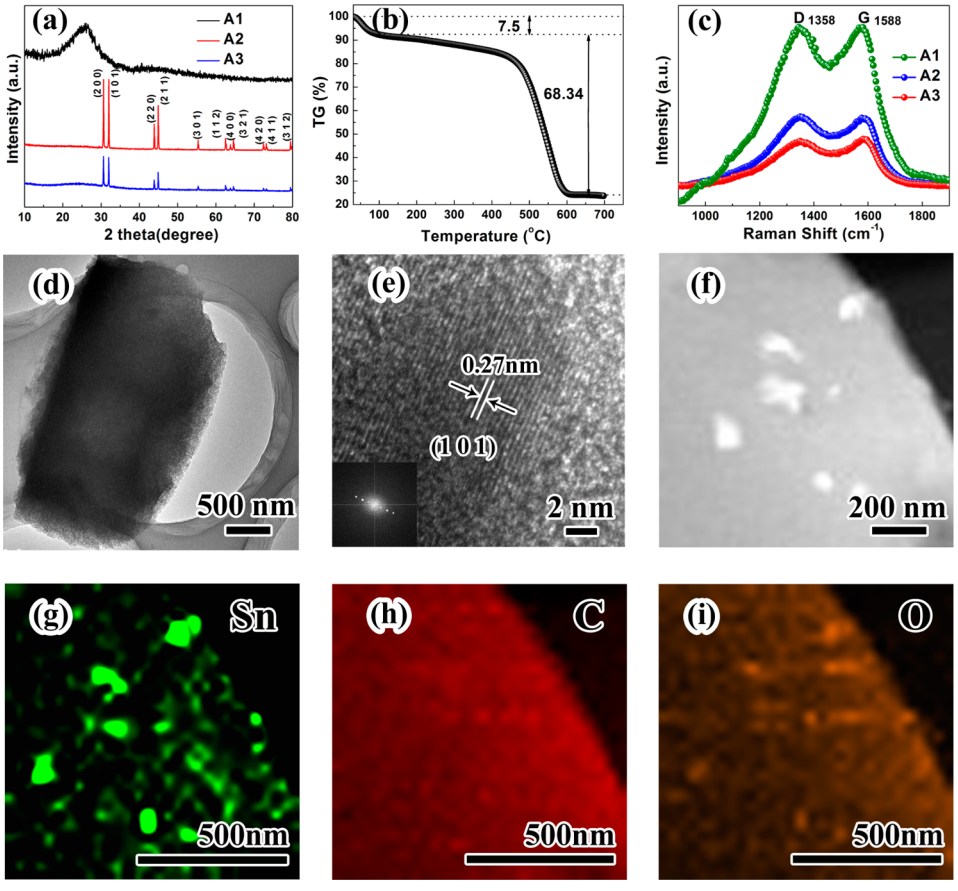

Figure 3. (a) XRD patterns of the as-prepared samples. (b) TGA curve of sample A3. (c) Raman spectrum of the as-prepared samples. (d) TEM image of sample A3. (e) HRTEM image of sample A3 and the corresponding FFT image (inset). (f) STEM image of sample A3 and the corresponding elemental mappings of tin (g) and carbon (h), respectively.

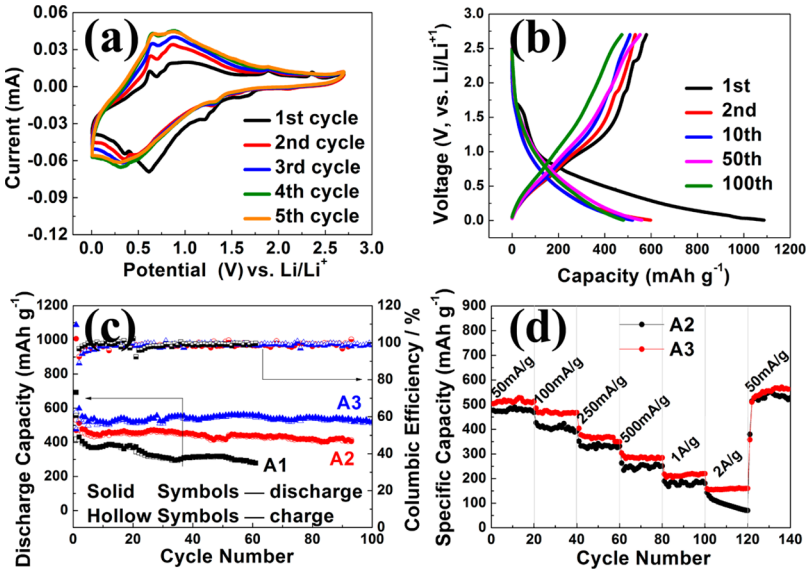

Figure 4. Electrochemical properties of the as-prepared samples. (a) CV curves of sample A3 scanned between 0.005 and 2.7 V at a rate of 0.1 mV s^{-1}. (b) Charge/discharge profiles of sample A3 at different cycles with a current densities of 50 mA g^{-1}. (c) Cycling performance and Coulombic efficiency of samples A1−A3 at a 50 mA g^{-1} current density. (d) Rate performance of samples A2 and A3.

Figure 3a represents the XRD patterns of the as-prepared samples. Only one broad peak centered at 25° was observed in sample A1, which was indicative of amorphous carbon. For samples A2 and A3, all of the intense peaks can be matched well with pure tin (JCPDS card no. 65-0296). According to the Scherrer formula ($D = k\lambda/\beta \cos \theta$), it is a fact that the larger the full width at half-maximum (β), the smaller the particle size (D). The particle size of sample A3 is smaller than that of sample A2 by comparing the β values of samples A2 and A3 from the XRD data. It can be explained that the PS film wrapped on the surface prohibits tin particle growth during pyrolysis.

TGA was carried out in air to quantify the carbon and tin contents in the Sn@C composite (sample A3). As shown in Figure 3b, the 7.5 wt % weight loss observed up to about 100 °C in the TGA curve is ascribed to dissipation of adsorbed water and air. Subsequently, the strong weight loss of 68.34% in the 100−700 °C range is a combination of the oxidation reactions of carbon and tin. After the temperature rose to 700 °C, all carbon and tin particles in the Sn@C composite have converted to CO_2 and SnO_2, respectively. According to the TGA results, the tin content in the Sn@C composite is calculated to be 26.5%, while it is 28.8% in sample A2 (Figure S1 in the Supporting Information, SI). The tin content in the Sn@C composite must be related to the biosorption capacity, which is affected by many kinds of environmental conditions, such as the solution concentration, pH value, and biological species.[49,50]

Raman spectroscopy is a significant technique for characterizing the quality of the carbon materials. In the Raman spectra (Figure 3c), all samples exhibited two main peaks at around 1358 and 1588 cm^{-1}, which can be assigned as the D peak for the disordered structure of carbon and the G peak for the graphite structure, respectively.[51] For sample A3, the intensity ratio of I_D/I_G is approximately 0.97, smaller than that of samples A1 and A2 (about 1.0), illustrating a higher degree of graphitization in sample A3. The result indicates that the PS coating layer favors the formation of graphitized carbon during the calcination process.

TEM examination was further performed to depict the elaborate microstructure of the Sn@C sample (A3). TEM (Figure 3d) and HRTEM (Figure 3e) images show that the Sn@C composite are constructed from tin particles dispersing in the porous carbon matrix, in which the tin particle size is 20−30 nm. The HRTEM image (Figure S2c in the SI) shows that the carbon matrix is composed of partially graphitized and amorphous components. Meanwhile, the obtained composite was estimated to have a high specific surface area value (326.89 m^2 g^{-1}) by BET measurement (Table S2 in the SI), which is consistent with the TEM images (Figure 3d) showing the existence of pores. The distinct lattice stripes in the HRTEM image (Figure 3e) and the corresponding fast Fourier transform (FFT) image (inset in Figure 3e) reveal that the tin particles are well-crystallized, and the distinct fringe space of about 0.27 nm can be indexed to (101) planes of tetragonal tin. Figure 3f shows a scanning transmission electron microscopy (STEM) image of a representative Sn@C sample. To further confirm the dispersion of tin, elemental mapping was carried out over the region in Figure 3f. The mapping of tin (Figure 3g) and carbon (Figure 3h) corroborate the fact that tin is indeed dispersed into the biological carbon host, which authentically confirms the previous results of XRD and SEM.

Figure 4 shows the electrochemical performance of the as-prepared samples as the anode materials of LIBs. All electrochemical capacities have been calculated on the total mass of the composites. Figure 4a displays CV curves of the Sn@C sample (A3) in the voltage range of 0.005−2.7 V at a scanning rate of 0.1 mV s^{-1}. During the first cathodic sweep, the peak at 0.32 V is obviously attributed to the formation of Li_xSn alloys, and the series of peaks ranging from 0.5 to 1.7 V are due to the complicated formation of a solid electrolyte interface (SEI) layer on the surface of both tin nanoparticles and the carbon matrix.[3] In the subsequent sweeps, two reduction peaks are observed at 0.30 and 0.49 V, which are ascribed to lithium alloying with tin forming Li_xSn alloys, while the oxidation peaks at 0.65 and 0.87 V are associated with the reversible delithiation processes of lithium from different kinds of Li_xSn alloys and the broad background is related to Li^+

extraction from carbon shells. Furthermore, the absence of reduction peaks at 1.05 or 1.55 V associated with catalytic decomposition of the electrolyte implies that tin was encapsulated in carbon matrixes.[52,53] Furthermore, the two oxidation peaks around 1.9 and 2.3 V must be attributed to the impurity substances derived from the biotemplate itself because *S. platensis* contains many mineral elements, such as iron (Fe), magnesium (Mg), calcium (Ca), and so forth.[40] The galvanostatic charge/discharge profiles of sample A3 at a current density of 50 mA g^{-1} are presented in Figure 4b. It is clearly demonstrated that the first discharge and charge capacities are 1087.6 and 579.6 mAh g^{-1} of the Sn@C composite electrode (A3) with a low coulombic efficiency of 53.3%. Compared to the theoretical capacity of metal tin (992 mAh g^{-1}), the extra discharge capacity of the Sn@C composite is mainly attributed to decomposition of the electrolyte with SEI formation. The initial discharge curve exhibits a long slope from around 1.0 to 0 V accompanying two small plateaus located at 0.6 and 0.32 V, which can be assigned to formation of the SEI film and alloying of lithium with tin, respectively. The discovery is basically consistent with the CV curves shown above. Slow shrinkage of the charge/discharge curves after the first cycle demonstrates good cycling stability.

The cycling performance of the Sn@C composite and control samples at a current density of 50 mA g^{-1} is shown in Figure 4c. Among the tested anodes, the A1 anode shows the lowest capacity and decreases after 20 cycles, whereas the A3 anode exhibits the best electrochemical performance with enhanced capacity retention. After 90 cycles, sample A3 can still be stable at a capacity of 541 mAh g^{-1}, while sample A2 can only deliver a lithium capacity of 424 mAh g^{-1}. For Sn@C composites, the mass loading of electrode materials is about 1 mg cm^{-2} for the 20-μm-thick electrode, so the corresponding volumetric capacity of sample A3 is calculated to be ~270 mAh cm^{-3} (see the SI for calculation details).[54] In addition to the first cycle, there is no serious capacity fading along with about 100 % efficiency, suggesting that the special nanostructure in the Sn@C (sample A3) composite can effectively encapsulate the metallic tin during repeated cycling, which ensures the excellent cyclic performance.

Figure 4d presents a comparison of the electrochemical performance between the A2 and A3 anodes at different current rates. The specific reversible capacity of the sample falls moderately with increasing current density. The Sn@C sample (A3) at different rates is superior to its counterpart (A2) in both the discharge capacity and cycling stability. At a high current density of 2A g^{-1}, sample A3 exhibits a stable discharge capacity of 155 mAh g^{-1}, while sample A2 decreases rapidly to 70 mAh g^{-1}. By returning to the initial 50 mA g^{-1} regime, both electrodes can even surpass the initial capacity, exhibiting satisfactory reversibility.

The microstructure evolution of the Sn@C composite after 100 charge/discharge cycles was investigated by TEM (Figure 5) to expound the excellent electrochemical performances. In contrast to the morphology of the fresh Sn@C composite anode in Figure 1b,c, no obvious morphology change was observed (Figure 5a). The cycled Sn@C sample keeps the original flake structure. However, the HRTEM image (Figure 5b) reveals that the diameter of the cycled tin particles is about 5 nm, which is much smaller than that of the pristine tin particles in the Sn@C composite. This phenomenon can be ascribed to pulverization of metallic tin and the buffering effect of the carbon matrix.[55] During the Li^+ insertion and extraction

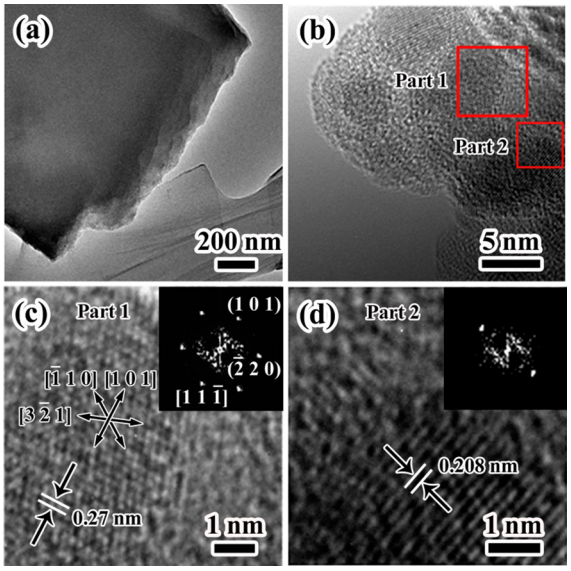

Figure 5. (a) TEM and (b) HRTEM images of the Sn@C composite charged to 2.7 V after 100 cycles at a 50 mA g^{-1} current density. Parts c and d are the amplified images of parts 1 and 2 in part b.

process, tin particles were expanded and pulverized repeatedly. Meanwhile, the rigid and elastic carbon matrix could compensate for expansion and prevent the structure from serious pulverization. Although the tin particles are gradually pulverized into smaller particles, the active materials are still anchored in the carbon matrix and retain good contact with the current collector, which results in the higher capacity and excellent cycling performance.

CONCLUSIONS

In summary, the Sn@C composite has been successfully synthesized through a facile and cost-effective biotemplating strategy exploiting the unique metal-ion biosorption behavior of microalgae, which is distinct from conventional biotemplate methods. Easily-reached, carbon-rich, and environmentally friendly *S. platensis* plays triple roles as the biotemplate, the biosorbent, and the carbon source in this technique. The tin particles with diameter of 20−30 nm are completely embedded in the porous carbon matrix of the Sn@C composite. FT-IR analysis illustrates that both the hydroxyl group of the alginate and the C−N stretching of proteins engage in the biosorption mechanisms of tin metal ions. Electrochemical measurements demonstrate that the Sn@C electrode has remarkable cycle stability and excellent cycling performance, which show a high potential for the anode material for LIBs. Furthermore, we believe that our green and facile strategy will not only extend the scope of the biotemplating synthesis of advanced functional materials but also provide an important reference for environmental protection and water purification.

ASSOCIATED CONTENT

Supporting Information

Information about chemicals used in the experiments and additional experimental data including TEM and HRTEM images, calculation of the volumetric capacity of sample A3, STEM image and elemental mapping of sample A2, BET and pore volume of obtained samples, and a TGA curve of sample A2. This material is available free of charge via the Internet at http://pubs.acs.org.

AUTHOR INFORMATION

Corresponding Author

*E-mail: msechem@zjut.edu.cn. Tel: +86-571-88320394.

Notes

The authors declare no competing financial interest.

ACKNOWLEDGMENTS

The authors acknowledge financial support by the National Natural Science Foundation of China (Grants 51002138 and 51172205), the Natural Science Foundation of Zhejiang Province (Grants LR13E020002 and LY13E020010), the Qianjiang Project of Zhejiang Province (Grant 2010R10029), the Scientific Research Foundation for the Returned Overseas Chinese Scholars (Grant 2010609), and New Century Excellent Talents in University (Grant NCET 111079).

REFERENCES

(1) Harman-Ware, A. E.; Morgan, T.; Wilson, M.; Crocker, M.; Zhang, J.; Liu, K.; Stork, J.; Debolt, S. Microalgae as a Renewable Fuel Source: Fast Pyrolysis of *Scenedesmus* Sp. *Renewable Energy* **2013**, *60*, 625−632.

(2) Xu, Y.; Liu, Q.; Zhu, Y.; Liu, Y.; Langrock, A.; Zachariah, M. R.; Wang, C. Uniform Nano-Sn/C Composite Anodes for Lithium Ion Batteries. *Nano Lett.* **2013**, *13*, 470−474.

(3) Duan, B. C.; Wang, W. K.; Zhao, H. L.; Xu, B.; Yuan, K. G.; Yang, Y. S. Nano-Sn/Mesoporous Carbon Parasitic Composite as Advanced Anode Material for Lithium-Ion Battery. *J. Electrochem. Soc.* **2012**, *159*, A2092−A2095.

(4) Derrien, G.; Hassoun, J.; Panero, S.; Scrosati, B. Nanostructured Sn−C Composite as an Advanced Anode Material in High-Performance Lithium-Ion Batteries. *Adv. Mater.* **2007**, *19*, 2336−2340.

(5) Zhang, W. M.; Hu, J. S.; Guo, Y. G.; Zheng, S. F.; Zhong, L. S.; Song, W. G.; Wan, L. J. Tin-nanoparticles Encapsulated in Elastic Hollow Carbon Spheres for High-Performance Anode Material in Lithium-Ion Batteries. *Adv. Mater.* **2008**, *20*, 1160−1165.

(6) Hassoun, J.; Derrien, G.; Panero, S.; Scrosati, B. A Nanostructured Sn−C Composite Lithium Battery Electrode with Unique Stability and High Electrochemical Performance. *Adv. Mater.* **2008**, *20*, 3169−3175.

(7) Lou, X. W.; Li, C. M.; Archer, L. A. Designed Synthesis of Coaxial SnO_2@Carbon Hollow Nanospheres for Highly Reversible Lithium Storage. *Adv. Mater.* **2009**, *21*, 2536−2539.

(8) Zhou, X. S.; Wan, L. J.; Guo, Y. G. Binding SnO_2 Nanocrystals in Nitrogen-Doped Graphene Sheets as Anode Materials for Lithium-Ion Batteries. *Adv. Mater.* **2013**, *25*, 2152−2157.

(9) Yu, Y.; Gu, L.; Zhu, C. B.; van Aken, P. A.; Maier, J. Tin Nanoparticles Encapsulated in Porous Multichannel Carbon Microtubes: Preparation by Single-Nozzle Electrospinning and Application as Anode Material for High-Performance Li-Based Batteries. *J .Am. Chem. Soc.* **2009**, *131*, 15984−15985.

(10) Wang, G.; Ma, Y. Q.; Liu, Z. Y.; Wu, J. N. Novel Highly Porous Sn−C Composite as High Performance Anode Material for Lithium-Ion Batteries. *Electrochim. Acta* **2012**, *65*, 275−279.

(11) Ni, W.; Wang, Y. B.; Xu, R. Formation of Sn@C Yolk-Shell Nanospheres and Core-Sheath Nanowires for Highly Reversible Lithium Storage. *Part. Part. Syst. Charact.* **2013**, *30*, 873−880.

(12) Elia, G. A.; Panero, S.; Savoini, A.; Scrosati, B.; Hassoun, J. Mechanically Milled, Nanostructured Sn−C Composite Anode for Lithium Ion Battery. *Electrochim. Acta* **2013**, *90*, 690−694.

(13) Wang, Y. G.; Li, B.; Zhang, C. L.; Tao, H.; Kang, S. F.; Jiang, S.; Li, X. Simple Synthesis of Metallic Sn Nanocrystals Embedded in Graphitic Ordered Mesoporous Carbon Walls as Superior Anode Materials for Lithium Ion Batteries. *J. Power Sources* **2012**, *219*, 89−93.

(14) Chen, J. Z.; Yang, L.; Fang, S. H.; Hirano, S. I. Ordered Mesoporous Sn−C Composite as an Anode Material for Lithium Ion Batteries. *Electrochem. Commun.* **2011**, *13*, 848−851.

(15) Yu, Y. H.; Yang, Q.; Teng, D. H.; Yang, X. P.; Ryu, S. Reticular Sn Nanoparticle-Dispersed PAN-Based Carbon Nanofibers for Anode Material in Rechargeable Lithium-Ion Batteries. *Electrochem. Commun.* **2010**, *12*, 1187−1190.

(16) Hsu, K. C.; Liu, C. E.; Chen, P. C.; Lee, C. Y.; Chiu, H. T. One-Step Vapor-Solid Reaction Growth of Sn@C Core-Shell Nanowires as an Anode Material for Li-Ion Batteries. *J. Mater. Chem.* **2012**, *22*, 21533−21539.

(17) Lee, K. T.; Jung, Y. S.; Oh, S. M. Synthesis of Tin-Encapsulated Spherical Hollow Carbon for Anode Material in Lithium Secondary Batteries. *J. Am. Chem. Soc.* **2003**, *125*, 5652−5653.

(18) Chen, J. J. Recent Progress in Advanced Materials for Lithium Ion Batteries. *Materials* **2013**, *6*, 156−183.

(19) Lupu, C.; Mao, J. G.; Rabalais, J. W.; Guloy, A. M.; Richardson, J. W. X-ray and Neutron Diffraction Studies on "$Li_{4.4}Sn$". *Inorg. Chem.* **2003**, *42*, 3765−3771.

(20) Chen, S.; Wang, Y.; Ahn, H.; Wang, G. Microwave Hydrothermal Synthesis of High Performance Tin-Graphene Nanocomposites for Lithium Ion Batteries. *J. Power Sources* **2012**, *216*, 22−27.

(21) Hou, X. Y.; Jiang, H.; Hu, Y. J.; Li, Y. F.; Huo, J. C.; Li, C. Z. In Situ Deposition of Hierarchical Architecture Assembly from Sn-Filled CNTs for Lithium-Ion Batteries. *ACS Appl. Mater. Interfaces* **2013**, *5*, 6672−6677.

(22) Xue, L. J.; Xu, Y. F.; Huang, L.; Ke, F. S.; He, Y.; Wang, Y. X.; Wei, G. Z.; Li, J. T.; Sun, S. G. Lithium Storage Performance and Interfacial Processes of Three Dimensional Porous Sn−Co Alloy Electrodes for Lithium-Ion Batteries. *Electrochim. Acta* **2011**, *56*, 5979−5987.

(23) Kim, G. P.; Lee, J. K.; Lee, Y. J.; Lee, J. H.; Baeck, S. H. Synthesis of Tin−Carbon Composite by RF (Resorcinol−Formaldehyde) Sol Method and Their Applications as Lithium Battery Anodes. *J. Nanosci. Nanotechnol.* **2008**, *8*, 5475−5478.

(24) Hwang, J.; Woo, S. H.; Shim, J.; Jo, C.; Lee, K. T.; Lee, J. One-Pot Synthesis of Tin-Embedded Carbon/Silica Nanocomposites for Anode Materials in Lithium-Ion Batteries. *ACS Nano* **2013**, *7*, 1036−1044.

(25) Zou, Y. Q.; Wang, Y. Sn@CNT Nanostructures Rooted in Graphene with High and Fast Li-Storage Capacities. *ACS Nano* **2011**, *5*, 8108−8114.

(26) Wang, Y.; Wu, M.; Jiao, Z.; Lee, J. Y. Sn@CNT and Sn@C@CNT Nanostructures for Superior Reversible Lithium Ion Storage. *Chem. Mater.* **2009**, *21*, 3210−3215.

(27) Deng, D.; Lee, J. Y. Reversible Storage of Lithium in a Rambutan-Like Tin−Carbon Electrode. *Angew. Chem., Int. Ed.* **2009**, *48*, 1660−1663.

(28) Deng, D.; Lee, J. Y. Direct Fabrication of Double-Rough Chestnut-Like Multifunctional Sn@C Composites on Copper Foil: Lotus Effect and Lithium Ion Storage Properties. *J. Mater. Chem.* **2010**, *20*, 8045−8049.

(29) Luo, B.; Wang, B.; Liang, M. H.; Ning, J.; Li, X. L.; Zhi, L. J. Reduced Graphene Oxide-Mediated Growth of Uniform Tin-Core/Carbon-Sheath Coaxial Nanocables with Enhanced Lithium Ion Storage Properties. *Adv. Mater.* **2012**, *24*, 1405−1409.

(30) Marcinek, A.; Hardwick, L. J.; Richardson, T. J.; Song, X.; Kostecki, R. Microwave Plasma Chemical Vapor Deposition of Nano-Structured Sn/C Composite Thin-Film Anodes for Li-Ion Batteries. *J. Power Sources* **2007**, *173*, 965−971.

(31) Yu, Y.; Gu, L.; Wang, C. L.; Dhanabalan, A.; van Aken, P. A.; Maier, J. Encapsulation of Sn@Carbon Nanoparticles in Bamboo-like Hollow Carbon Nanofibers as an Anode Material in Lithium-Based Batteries. *Angew. Chem., Int. Ed.* **2009**, *48*, 6485−6489.

(32) Park, C. M.; Kim, J. H.; Kim, H.; Sohn, H. J. Li-Alloy Based Anode Materials for Li Secondary Batteries. *Chem. Soc. Rev.* **2010**, *39*, 3115−3141.

(33) Zhao, H. P.; Jiang, C. Y.; He, X. M.; Ren, J. G.; Wan, C. R. Advanced Structures in Electrodeposited Tin Base Anodes for Lithium Ion Batteries. *Electrochim. Acta* **2007**, *52*, 7820−7826.

(34) Ramimoghadam, D.; Bin Hussein, M. Z.; Taufiq-Yap, Y. H. Hydrothermal Synthesis of Zinc Oxide Nanoparticles Using Rice as Soft Biotemplate. *Chem. Cent. J.* **2013**, 7.
(35) Tao, X. Y.; Du, J.; Li, Y. P.; Yang, Y. C.; Fan, Z.; Gan, Y. P.; Huang, H.; Zhang, W. K.; Dong, L. X.; Li, X. D. TaC Nanowire/Activated Carbon Microfiber Hybrid Structures from Bamboo Fibers. *Adv. Energy Mater.* **2011**, *1*, 534−539.
(36) Qiu, Z.; Huang, H.; Du, J.; Fen, T.; Zhang, W. K.; Gan, Y. P.; Tao, X. Y. NbC Nanowire-Supported Pt Nanoparticles as a High Performance Catalyst for Methanol Electrooxidation. *J. Phys. Chem. C* **2013**, *117*, 13770−13775.
(37) Tao, X. Y.; Li, Y. P.; Du, J.; Xia, Y.; Yang, Y. C.; Huang, H.; Gan, Y. P.; Zhang, W. K.; Li, X. D. A Generic Bamboo-Based Carbothermal Method for Preparing Carbide (SiC,B_4C, TiC, TaC, NbC, $Ti_xNb_{1-x}C$, and$Ta_xNb_{1-x}C$) Nanowires. *J. Mater. Chem.* **2011**, *21*, 9095−9102.
(38) Xia, Y.; Zhang, W. K.; Xiao, Z.; Huang, H.; Zeng, H. J.; Chen, X. R.; Chen, F.; Gan, Y. P.; Tao, X. Y. Biotemplated Fabrication of Hierarchically Porous NiO/C Composite from Lotus Pollen Grains for Lithium-Ion Batteries. *J. Mater. Chem.* **2012**, *22*, 9209−9215.
(39) Tao, X. Y.; Dong, L. X.; Wang, X. N.; Zhang, W. K.; Nelson, B. J.; Li, X. D. B_4C-Nanowires/Carbon-Microfiber Hybrid Structures and Composites from Cotton T-shirts. *Adv. Mater.* **2010**, *22*, 2055−2059.
(40) Xia, Y.; Zhang, W. K.; Huang, H.; Gan, Y. P.; Xiao, Z.; Qian, L. C.; Tao, X. Y. Biotemplating of Phosphate Hierarchical Rechargeable $LiFePO_4$/C Spirulina Microstructures. *J. Mater. Chem.* **2011**, *21*, 6498−6501.
(41) Xia, Y.; Xiao, Z.; Dou, X.; Huang, H.; Lu, X. H.; Yan, R. J.; Gan, Y. P.; Zhu, W. J.; Tu, J. P.; Zhang, W. K.; Tao, X. Y. Green and Facile Fabrication of Hollow Porous MnO/C Microspheres from Microalgae for Lithium-Ion Batteries. *ACS Nano* **2013**, *7*, 7083−7092.
(42) Tao, X. Y.; Du, J.; Yang, Y. C.; Li, Y. P.; Xia, Y.; Gan, Y. P.; Huang, H.; Zhang, W. K.; Li, X. D. TiC Nanorods Derived from Cotton Fibers: Chloride-Assisted VLS Growth, Structure, and Mechanical Properties. *Cryst. Growth Des.* **2011**, *11*, 4422−4426.
(43) Sandau, E.; Sandau, P.; Pulz, O. Heavy Metal Sorption by Microalgae. *Acta Biotechnol.* **1996**, *16*, 227−235.
(44) Cho, H. J.; Baek, K.; Jeon, J. K.; Park, S. H.; Suh, D. J.; Park, Y. K. Removal Characteristics of Copper by Marine Macro-Algae-Derived Chars. *Chem. Eng. J.* **2013**, *217*, 205−211.
(45) Kumar, Y. P.; King, P.; Prasad, V. S. R. K. Adsorption of Zinc From Aqueous Solution Using Marine Green Algae—Ulva Fasciata Sp. *Chem. Eng. J.* **2007**, *129*, 161−166.
(46) Fourest, E.; Volesky, B. Contribution of Sulfonate Groups and Alginate to Heavy Metal Biosorption by the Dry Biomass of Sargassum Fluitans. *Environ. Sci. Technol.* **1996**, *30*, 277−282.
(47) Schiewer, S.; Volesky, B. Biosorption Processes for Heavy Metal Removal. *Environmental Microbe−Metal Interactions*; ASM Press: Washington, DC, 2000; pp 329−362.
(48) Arief, V. O.; Trilestari, K.; Sunarso, J.; Indraswati, N.; Ismadji, S. Recent Progress on Biosorption of Heavy Metals from Liquids Using Low Cost Biosorbents: Characterization, Biosorption Parameters and Mechanism Studies. *Clean: Soil, Air, Water* **2008**, *36*, 937−962.
(49) Ho, Y. C.; Mi, F. L.; Sung, H. W.; Kuo, P. L. Heparin-Functionalized Chitosan−Alginate Scaffolds for Controlled Release of Growth Factor. *Int. J. Pharm.* **2009**, *376*, 69−75.
(50) Ata, A.; Nalcaci, O. O.; Ovez, B. Macro Algae Gracilaria Verrucosa as a Biosorbent: A Study of Sorption Mechanisms. *Algal Res.* **2012**, *1*, 194−204.
(51) Tao, X. Y.; Zhang, X. B.; Zhang, L.; Cheng, J. P.; Liu, F.; Luo, J. H.; Luo, Z. Q.; Geise, H. J. Synthesis of Multi-Branched Porous Carbon Nanofibers and Their Application in Electrochemical Double-Layer Capacitors. *Carbon* **2006**, *44*, 1425−1428.
(52) Luo, B.; Wang, B.; Li, X. L.; Jia, Y. Y.; Liang, M. H.; Zhi, L. J. Graphene-Confined Sn Nanosheets with Enhanced Lithium Storage Capability (**2012**, *24*, 3538). *Adv. Mater.* **2012**, *24*, 5525−5525.
(53) Song, X. F. A Hierarchical Hybrid Design for High Performance Tin Based Li-Ion Battery Anodes. *Nanotechnology* **2013**, 24.
(54) Chen, J. J.; Yano, K. Highly Monodispersed Tin Oxide/Mesoporous Starbust Carbon Composite as High-Performance Li-Ion Battery Anode. *ACS Appl. Mater. Interfaces* **2013**, *5*, 7682−7687.
(55) Liang, S.; Zhu, X.; Lian, P.; Yang, W.; Wang, H. Superior Cycle Performance of Sn@C/Graphene Nanocomposite as an Anode Material for Lithium-Ion Batteries. *J. Solid State Chem.* **2011**, *184*, 1400−1404.